Mon. Not. R. Astron. Soc. **000**, ??–?? (2007) Printed 5 February 2008 (MN LATEX style file v2.2)

# A longer *XMM-Newton* look at I Zwicky 1: physical conditions and variability of the ionised absorbers

E. Costantini [1,2⋆], L.C. Gallo[3,4], W.N. Brandt[5], A.C. Fabian[6] and Th. Boller[4]
[1] *SRON National Institute for Space Research, Sorbonnelaan 2, 3584 CA Utrecht, The Netherlands*
[2] *Astronomical Institute, Utrecht University, P.O. Box 80000, 3508 TA, Utrecht, The Netherlands*
[3] *SUPA, School of Physics and Astronomy, University of St. Andrews, North Haugh, St. Andrews, Fife KY16 9SS*
[4] *Max-Planck Institute füer extraterrestrische Physik, Giessenbachstr 1, 45748, Garching bei Muenchen, Germany*
[5] *Department of Astronomy and Astrophysics, Pennsylvania State University, University Park, PA 16802*
[6] *Institute of Astronomy, University of Cambridge, Madingley Road, Cambridge CB3 0HA*

arXiv:astro-ph/0702553v1 21 Feb 2007

Received / Accepted

**ABSTRACT**

We present a spectral analysis of the narrow-line Seyfert 1 galaxy I Zwicky 1, focusing on the characteristics of the ionised absorbers as observed with *XMM-Newton* in 2005. The soft X-ray spectrum shows absorption by two components of ionised gas with a similar column density ($N_{\rm H} \sim 10^{21}$ cm$^{-2}$) and ionisation parameters $\log \xi \sim 0$ and 2.5. Comparing this observation with a 2002 *XMM-Newton* data set, we see a clear anti-correlation between the X-ray ionisation parameter $\xi_{\rm X}$ and the $0.1-10$ keV luminosity. Viable explanations for this effect include transient clouds or filaments crossing the line of sight in a complex geometry or a gas observed in non-equilibrium. The outflow velocity of the X-ray low-ionisation absorber is consistent with the outflow of the UV absorber detected in a past Hubble Space Telescope observation. In addition, the ionic column densities of C IV and N V derived from the X-ray model are consistent with the UV values. This suggests that the low-ionisation outflowing gas may survive for many years, despite large changes in flux, and that there is a tight connection between the X-ray and UV absorbers that can only be confirmed with a simultaneous UV and X-ray observation.

**Key words:** Galaxies: individual: I Zw 1 – Galaxies: Seyfert – quasars: absorption lines – Ultraviolet: galaxies – X-rays: galaxies

## 1 INTRODUCTION

About 50–70% of active galactic nuclei (AGN) display absorption by photoionised gas in their X-ray spectra (e.g. Reynolds 1997; George et al. 1998). With the advent of high energy resolution instruments, the study of the brightest sources has allowed us to detail the characteristics of such gas (e.g. Kaastra et al. 2002; Kaspi et al. 2002; Kraemer et al. 2005; Turner et al. 2005). Multiple components are often detected, differing in column density, ionisation and outflow velocity. At least some of the lower ionisation X-ray components most probably share the same location as the UV components (e.g. Turner et al. 2005; Costantini et al. 2007) as first suggested by Mathur et al. (1995). Variability studies point out the complex response of the ionised absorbers (also called warm absorbers) to central-source flux variations. A linear response of the ionisation parameter[1] of the gas component to the continuum change provides a constraint on the distance to the absorber (e.g. Netzer et al. 2002; Turner et al. 2005; Otani et al. 1996). A linear response gives a relatively intuitive picture of the geometry of the absorber as a thin slab of material in thermal equilibrium (either in clouds or filaments) exposed to the ionising flux. In other variability studies (e.g. NGC 4151, Kraemer et al. 2005) the gas does not obey this simple picture, suggesting instead that gas outflows often change direction along the line of sight in a unpredictable way.

I Zwicky 1 (I Zw 1) is a well-studied narrow-line Seyfert 1 galaxy (NLS1; see Vestergaard Wilkes 2001, and references therein) located at redshift $z$=0.06112±0.000015 (Condon et al. 1985). Since the time of ROSAT observations, I Zw 1 has been known to host intrinsic absorption

⋆ E-mail: e.costantini@sron.nl

[1] The ionisation parameter is defined as $\xi = L/nr^2$, where $L$ is the 1–1000 Ryd ionising luminosity, $n$ and $r$ are the density and the distance to the ionised gas.

in the X-ray band (Boller et al. 1996; Lawrence et al. 1997). From moderate-resolution ASCA data, Leighly (1999) could distinguish between a neutral component ($N_{\rm H} \sim 2.6 \times 10^{20}\,{\rm cm}^{-2}$) and an ionised absorber, typically highlighted, in lower resolution spectra, by the O VII and O VIII absorption edges. A similar spectral complexity was reported by Gallo et al. (2004), using *XMM-Newton* data. The presence of fast ($v_{\rm out} \sim -1870\,{\rm km\,s}^{-1}$) outflowing ionised gas was observed in the UV spectrum of I Zw 1 (using HST-FOS; Laor et al. 1997; Crenshaw et al. 1999), through the analysis of the N V and C IV absorption troughs. FUSE observed the O VI absorption troughs, which displayed multiple components (Kriss 2002).

This paper is one in a series devoted to a long *XMM-Newton* observation of I Zw 1. In the present study we focus on the soft X-ray absorbers, discussing the physical picture returned by the long-term variability of this gas and its connection with the UV absorbers. Other works deal with the continuum emission and the variable iron K$\alpha$ line (Gallo et al. 2007a, hereinafter Paper I), and with the spectral variability analysis (Gallo et al. 2007b).

The paper is organised as follows. In Sect. 2 the main features of the data reduction and the EPIC-pn analysis (described in detail in Paper I) are summarised. Sect. 3 is devoted to the analysis of the RGS data and the modelling of the spectral features in I Zw 1. In Sect. 4 we discuss our results and in Sect. 5 we present the conclusions. The cosmological parameters used are $H_0$=70 ${\rm km\,s}^{-1}{\rm Mpc}^{-1}$, $\Omega_m$=0.3, and $\Omega_\Lambda$=0.7. The quoted errors are at 90% confidence for one interesting parameter, unless otherwise stated. The assumed Galactic column density is $N_{\rm H} = 5.07 \times 10^{20}\,{\rm cm}^{-2}$ (Elvis et al. 1989).

## 2 THE DATA ANALYSIS

I Zw 1 was observed on July 18-19 2005 (rev. 1027) for 85.5 ks. Data from the three EPIC cameras MOS (Turner et al. 2001) and pn (Strüder et al. 2001), the high resolution spectrometer RGS (den Herder et al. 2001) and the optical monitor (OM, Mason et al. 2001) were successfully gathered. After filtering high-background intervals, the net exposure time was $\sim$ 58 ks for EPIC-pn and $\sim$ 84 ks for RGS. The event files for each instrument were created with the newest SAS pipeline (ver. 7.0). This version of SAS benefits from improved calibrations of RGS time-dependent effective area, absolute RGS flux and bad-pixel location[2]. The discrepancies between EPIC-pn and RGS are of the order of 10%, similar as for EPIC-MOS when compared to EPIC-pn.

The spectral analysis of the soft X-ray spectrum was carried out using the fitting package SPEX[3] (ver. 2.0). We rebinned the RGS data to reach a signal-to-noise ratio (S/N) of $\sim$9 over the whole energy band. During the observation the source shows two different average flux states, which differ approximately by 44% and 36% in the soft (0.3–2 keV) and hard (2–10 keV) energy bands, respectively. The flux changes after $\sim$27 ks since the start of the observation and happens on a dynamical time scale of $\sim$5 ks. The flux variations in the soft and hard X-ray bands show similar trends (see Fig. 3 of Paper I). We will study the effect of the flux change on the RGS spectrum in Sect. 3.

The data from the EPIC-pn camera were used to constrain the broad-band spectrum. The modelling of the continuum is described in full detail in Paper I. For the purpose of studying any narrow absorption/emission features in the RGS band, the detailed broad-band continuum shape is not crucial. For simplicity, here we describe the continuum with a broken power-law, which fits the data well (Tab.1). However in Sect. 3.1, we test our results for different continua.

## 3 THE SOFT ENERGY SPECTRUM

The RGS spectrum shows the signatures of absorption, especially around the O VII and O VIII absorption edges. In order to fit a photoionised absorber, we used the SPEX model XABS, which interpolates on a fine grid the $N_{\rm H}$ and $\log\xi$ values. The ionisation balance is constructed from the spectral energy distribution (SED) specific for the source (solid curve in Fig. 1), using Cloudy (Ferland 2004). Here and in the following analysis, the SED definition takes advantage of the simultaneous EPIC-pn and OM data. The OM data were collected in fast-mode (see Paper 1) in the $U$ (3440Å), UVW1 (2910Å), UVW2 (2120Å) and UVM2 (2310Å) filters. We considered the average flux for each filter. By interpolation, we obtained the flux at 2500 Å that we used in constructing the SED. Interpolating the OM points was mandatory in order to compare consistently the ionisation balance obtained with this SED with the one obtained from a previous *XMM-Newton* data set for which only one OM filter was available (Sect. 3.2). An adopted SED will always have a degree of uncertainty, when dealing with limited multiwavelength data. When comparing SEDs of different flux states of the same object it is important to consistently compare the resulting ionisation balances. The SED of 2002 was likely similar to 2005 in the UV regime, but in 2002 only one OM filter was available. This would make any "reconstruction" of the 2002 SED highly arbitrary. Therefore the only way to consistently compare the SEDs at the two epochs is to interpolate the 2005 OM points. Beyond the optical band, we used a standard AGN continuum, characterised by relatively low emission at longer wavelengths, as defined in Cloudy. The host galaxy of I Zw 1 is indeed very luminous both in the far-infrared and in the infrared (Halpern Oke 1987). In the long-wavelength band it is important to avoid dust contamination of the nuclear emission by the host galaxy. In general, an overestimation of the infrared radiation may lead to an incorrect ionisation balance determination (see e.g. Ferland et al. 2002).

Tunable parameters of the XABS model, in addition to $N_{\rm H}$ and $\log\xi$, are the root mean squared width of the absorption lines, the outflow velocity, the line-of-sight covering factor of the gas and the elemental abundances. We fixed the covering factor to unity and we assumed solar abundances (Anders Grevesse 1989) throughout the analysis.

In Tab. 1 we list the best-fit parameters for the absorbers in I Zw 1 as measured by the RGS and, for consistency, with

[2] For further details refer to http://xmm.vilspa.esa.es/external/xmm_user_support/usersgroup/20060518/index.shtml.

[3] http://www.sron.nl/divisions/hea/spex/version2.0/release/index.html

the lower resolution EPIC-pn data. The model parameters are always consistent between RGS and EPIC-pn. However, the higher energy resolution makes RGS more reliable for the modelling of narrow absorption features, and we will consider the physical parameters constrained with the RGS data for the discussion.

A warm absorber (hereinafter labelled 05a), with a column density $N_{\rm H} \sim 1.3 \times 10^{21}\,{\rm cm}^{-2}$ and an ionisation parameter $\log\xi \sim 0$ is highlighted in the RGS data especially by the blend of the O VII K absorption edge and the iron unresolved transition array (UTA). The gas is found to be outflowing at $\sim$1700 km s$^{-1}$. The widths of the lines are loosely constrained ($\sigma = 36 \pm 20\,{\rm km\,s}^{-1}$), but still consistent with the more accurate FUSE measurement of $30\pm5\,{\rm km\,s}^{-1}$ (G. Kriss, private communication). Additional ionised absorption is required to fit the region below the O VIII edge ($\lambda = 14.22$Å). The improvement of the fit after the inclusion of this second absorber is $\Delta\chi^2/\Delta\nu$=27/2, where $\nu$ is the number of degrees of freedom. The second gas component (hereinafter 05b) has a higher ionisation parameter ($\log\xi \sim 2.6$, Tab. 1) but a column density similar to the 05a component. We fixed the widths of the lines to the value for the lower ionisation component. The absorption lines of the higher ionisation component lie in a spectral region of lower resolution, and a possible outflow velocity is hard to quantify. The upper limit on the outflow velocity of the 05b component is $v_{\rm out} < 800\,{\rm km\,s}^{-1}$. Finally, a neutral component, identified by an O I edge at the redshift of the source and with $N_{\rm H} \sim 1.5 \times 10^{20}\,{\rm cm}^{-2}$, is required by the data. The addition of this component improves the fit by $\Delta\chi^2/\Delta\nu$=19/1 (where the column density is the additional parameter). In Fig. 2, we plot the transmission of the neutral and warm gas components (upper panel), the observed RGS spectrum with the best-fit model (middle panel) and the residuals from the best fit (lower panel).

The above analysis refers to the total RGS spectrum. However (Sect. 2), the soft and hard energy bands undergo variations during the *XMM-Newton* pointing. Using the RGS data we further verified that only continuum changes are responsible for the overall variations in the source flux and not opacity variations of the ionised gas. We divided the RGS data into two time segments, corresponding to the higher ($\sim$30 ks long) and lower state ($\sim$40 ks). The higher state best fit does not vary significantly with respect to the average spectral fit, except for the normalisation and slope of the power law. We then used the higher flux state best-fit model (see above) as a template for the lower flux state and found that the neutral and warm absorbers do not vary within the uncertainties.

### 3.1 Other continuum models

In the present paper the continuum is represented by a simple broken power law. A discussion of the continuum models and their physical implications is given in Paper I. Here we test different continuum models only in order to assess the robustness of the warm-absorber parameters. We follow the same approach as in Sect. 3, the broad-band continuum is established using EPIC-pn and then applied to the RGS, in order to tune the warm absorbers' parameters.

First we used a power law plus modified black-body emission and neutral absorption (both from the host galaxy and from the Milky Way). In the black-body model the effects of Compton scattering are considered (Kaastra Barr 1989). A black-body temperature of $\sim$0.13 keV is required to fit the low energies. Without any warm absorber the resulting reduced $\chi^2$ ($\chi^2/\nu$) is $\sim$1.32. The addition of one warm absorber (two additional free parameters) improves the fit by $\Delta\chi^2$=93. A second component improves the fit by another $\Delta\chi^2/\Delta\nu = 23/2$. The final model has a higher black body temperature, $kT$ $\sim$0.2 keV (see Paper I for a discussion). The total black-body luminosity is however very low ($\sim 2.7 \times 10^{42}\,{\rm erg\,s}^{-1}$) compared to the dominant power law component ($\sim 1.3 \times 10^{43}\,{\rm erg\,s}^{-1}$) in the 0.3–10 keV band. The warm absorbers parameters do not differ within the er-

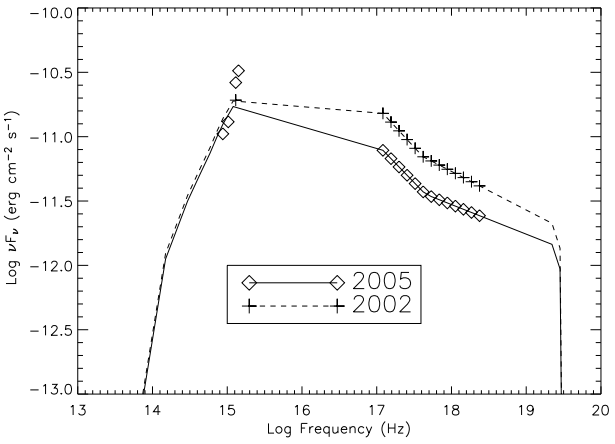


**Figure 1.** The adopted SEDs for the 05 observation (solid line) and 02 observation (dashed line). The X-ray shape of the SED is based on the EPIC-pn data, while the point at 2500Å is derived by interpolation of the OM data points. The 05 OM points (open diamonds around $10^{15}$ Hz) were interpolated to the same wavelength measurement of 02, in order to compare consistently the 05 SED with the 02 one, for which data from only one OM filter was available.

**Table 1.** 2005 best-fit model parameters for RGS and PN. Fluxes are in units of $10^{-12}$ erg s$^{-1}$ cm$^{-2}$, unabsorbed luminosity in units of $10^{43}$ erg s$^{-1}$. Component 1: broken power law, 2: neutral absorber, 3,4: warm absorbers. All emission components are modified by Galactic photoelectric absorption.

| comp. | param. | R1+R2 | PN |
|---|---|---|---|
| 1 | $\Gamma_1$ | 2.5±0.1 | 2.58±0.05 |
| | $\Gamma_2$ | ... | 2.21±0.05 |
| | $E_{\rm break}$ (keV) | ... | 2.0±0.1 |
| 2 | $N_{\rm H}$ ($10^{20}$ cm$^{-2}$) | 1.7±1 | 1.5±0.4 |
| 3 | $N_{\rm H}$ ($10^{20}$ cm$^{-2}$) | 13±3 | 9±1 |
| | $\log\xi$ | 0.05±0.16 | 0.16±0.14 |
| | $v_{\rm out}$ (km s$^{-1}$) | –1700±400 | –1700 fix. |
| 4 | $N_{\rm H}$ ($10^{20}$ cm$^{-2}$) | 13±5 | 8±3 |
| | $\log\xi$ | 2.6±0.3 | 2.0±0.4 |
| | $\chi^2/\nu$ | 411/358 | 530/513 |
| | $F_{2-10\,{\rm keV}}$ | ... | 4.86±0.06 |
| | $F_{0.5-2\,{\rm keV}}$ | 5.0±0.3 | 5.13±0.07 |
| | $L_{2-10\,{\rm keV}}$ | ... | 4.50±0.06 |
| | $L_{0.5-2\,{\rm keV}}$ | 7.0±0.4 | 6.10±0.08 |

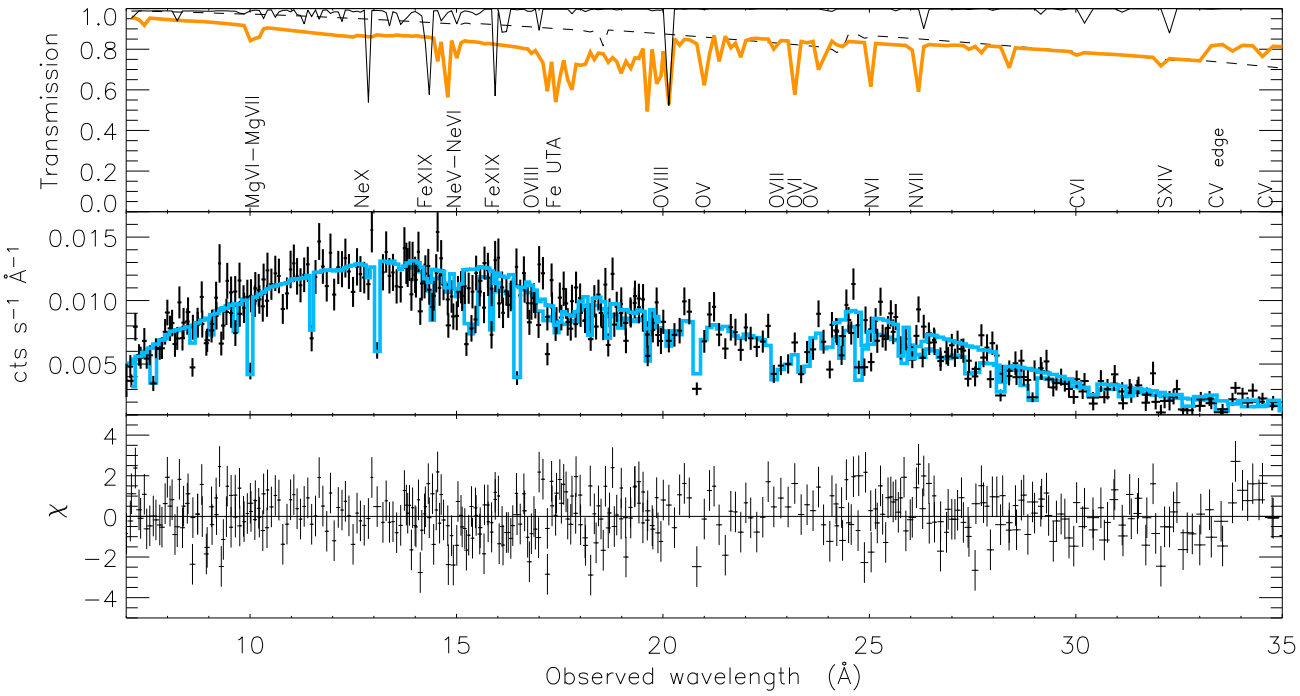


**Figure 2.** Upper panel: transmission models (convolved with the data resolution) of the neutral absorber (dashed line) and the ionised components for the 05 spectrum. Component 05a is displayed with the light line and 05b with the dark line. The most relevant transitions are also labelled. Middle panel: RGS data together with the best fit. Lower panel: residuals from the best-fit model.

rors from the ones listed in Tab. 1.

Next, we tested a relativistically blurred reflection model (Ross Fabian 2005). We fixed the parameters to the model values determined in Paper I, i.e. the disc inclination to 51°, its emissivity $\alpha = 2.5$ and inner radius to 5 gravitational radii. We assumed solar abundances for the disc material. A fit without any ionised absorption results in a $\chi^2/\nu$ of 1.56. This value decreases to 1.21, adding one warm absorber. A second warm absorber component again improves the fit, as in the previous cases ($\Delta\chi^2/\Delta\nu = 20/2$). Note that for this exercise we do not attempt any fit of the Fe K$\alpha$ line. The amount of reflected light with respect to the total luminosity budget is modest (few percent), resulting in a weak soft excess. We conclude that for the purpose of our study a simple broken-power law fit is acceptable.

### 3.2 The recent history of the absorbed X-ray spectrum

I Zw 1 was observed by *XMM-Newton* for the first time on June 22, 2002 (rev. 0464) for 20 ks (Gallo et al. 2004). At the time the source 2–10 keV flux was about 1.7 times higher than in the present observation and showed remarkable spectral complexity at low energies. In Fig. 3 we over-plot the two EPIC-pn data sets, but with the 2005 spectrum shifted up in order to best match the continuum during 2002. A qualitative inspection of the figure shows that the soft energies underwent the most dramatic changes between the two epochs (we refer to the 2005 and 2002 data sets as 05 and

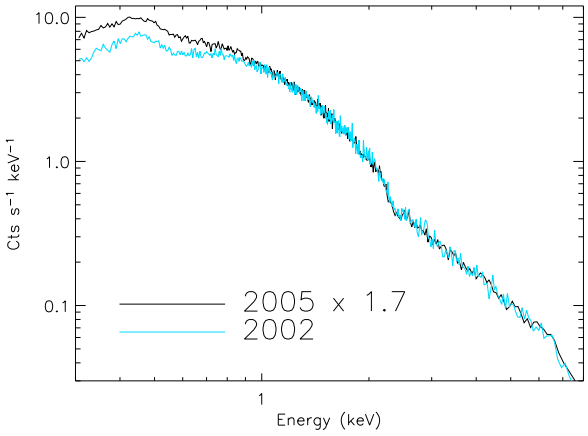


**Figure 3.** EPIC-pn spectra taken in 02 (light line) and 05 (dark line). The spectrum of 05 is multiplied by 1.7 to best match the hard continuum during 2002 and emphasises the low energy complex variability.

02, respectively). We reprocessed the 02 RGS and EPIC-pn data using SAS 7.0 and we focused the analysis mostly on the warm absorber. The RGS data were rebinned to reach a S/N ratio $\sim 9$ over most of the band. The best fit shows that the underlying continuum changed between 02 and 05 mostly in flux rather than shape, which is here again described by a simple broken power law (Tab. 2). The shape

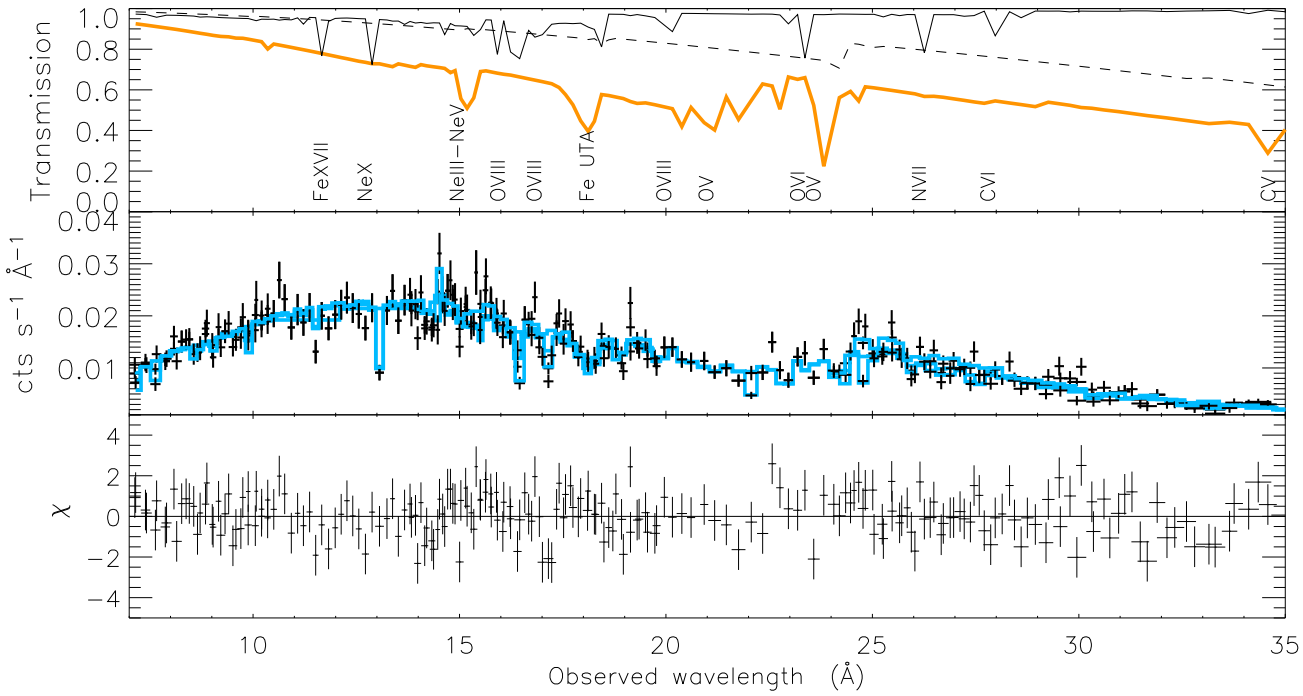


**Figure 4.** Upper panel: transmission models (convolved with the data resolution) of the neutral absorber (dashed line) and the ionised components for the 02 spectrum. Component 02a is displayed with the light line and 02b with the dark line. The most relevant transitions are also labelled. Middle panel: RGS data together with the best fit. Lower panel: residuals from the best fit.

of the ionising continuum was again constructed using the unabsorbed EPIC-pn continuum and the fluxes recorded in optical/UV by OM (dashed line in Fig. 1). In 02 only the OM-UVW2 filter was used. Similarly to the 05 data, in addition to the neutral gas, we find evidence for two ionised absorption components. The corresponding ionisation parameters are $\log\xi \sim -0.9$ and $\log\xi \sim 1.6$. We identify these two warm absorber components as 02a and 02b, respectively (Fig. 4). Interestingly, we find evidence that the 02a component outflows with a velocity similar to the 05a component ($v_{\rm out} \sim 1800\,{\rm km\,s^{-1}}$). The width of the lines is $\sigma = 67 \pm 50\,{\rm km\,s^{-1}}$. Going further back into the recent history of the X-ray absorbers of I Zw 1, we reanalysed the ASCA data obtained in 1995 (Leighly 1999). The continuum is once again well fitted by a broken power law with parameters comparable to the most recent 05 *XMM-Newton* spectra: $\Gamma_{\rm soft} = 2.58 \pm 0.07$, $\Gamma_{\rm hard} = 2.35 \pm 0.07$ and a break energy at $2.0 \pm 0.8\,{\rm keV}$. We confirm the presence of a neutral gas phase with column density $N_{\rm H} = 4 \pm 1 \times 10^{20}\,{\rm cm^{-2}}$, consistent with the values found with *XMM-Newton*.

For the ASCA data, simultaneous UV observations were unavailable; therefore a true SED could not be constructed. The ionising SED was then built using the ASCA continuum plus the same $\alpha_{\rm ox}$ [4] $= -1.25$ found in 05. We used this SED only to obtain a best fit that consistently accounted for the absorption features and then only considered the ionic column densities (and not the ionisation parameter) to compare with our *XMM-Newton* results.

As the ionisation parameter is dependent on the ionisation balance (i.e. the SED), a good way to compare warm absorbers produced by different (or incomplete) SEDs, is to evaluate the different elemental ionic column densities. In particular, iron is the most sensitive to changes in the ionisation of the gas (e.g. Behar et al. 2001). In Fig. 5, we plot the ionic column densities as a function of the ionisation stage of iron for each of the X-ray ionisation components detected in this source. The column densities are obtained from the XABS best-fit models. The relative errors are simply the scaled errors from the total hydrogen column densities of the XABS ionisation components. The 02 components are well separated: 02a peaks at Fe V, while 02b peaks at Fe XIV-Fe XVI. The 05a component has a relatively lower total column density (Tab. 1) and shares some ions with the 02a components. The 05b component displays the highest ionised iron transitions. The ASCA component (labelled 95) is more in the high ionisation region.

A possible second component in the ASCA spectrum would be difficult to detect. We verified that a higher ionisation component, with a column density of the order of $10^{21}\,{\rm cm^{-2}}$ would produce mostly lines (see Fig. 2, 4), which would be undetectable in the ASCA spectrum. A much less ionised gas peaking, say at Fe III-Fe V, would be easily confused with the neutral absorber.

[4] $\alpha_{\rm ox}$ is the spectral index between 2500 Å and 2 keV (Tananbaum et al. 1979).

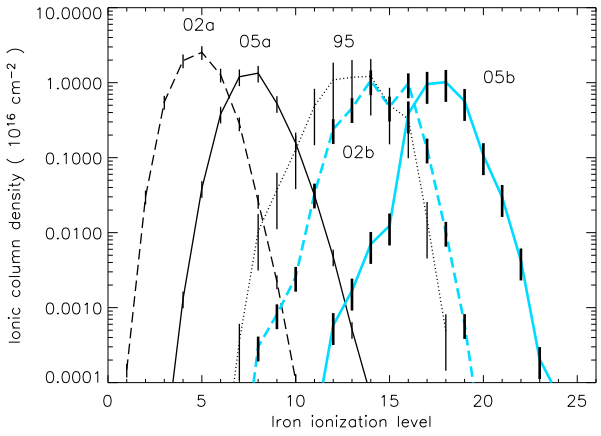


**Figure 5.** Ionic column density as a function of the ionisation level of iron in the warm absorber components detected in recent years by *XMM-Newton* (02a, 02b, 05a and 05b) and ASCA (95).

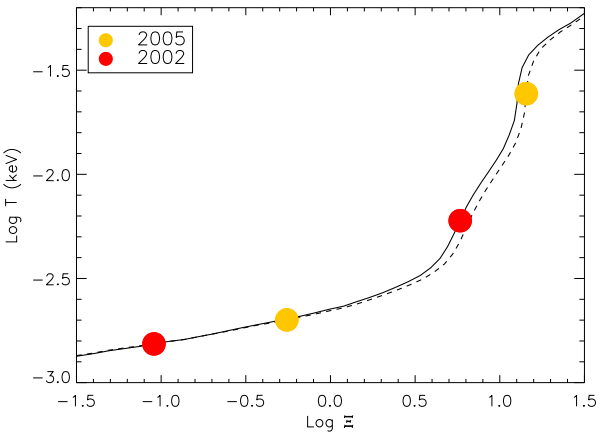


**Figure 6.** Stability curve for the 2002 (solid line) and 2005 (dashed line) observations. The dark circles represent the two ionised components detected in 2002, while the light circles represents the 2005 components. None of the components share the same pressure ionisation parameter.

**Table 2.** 2002 best-fit model parameters for RGS and PN. Fluxes are in units of $10^{-12}$ erg s$^{-1}$ cm$^{-2}$, unabsorbed luminosity in units of $10^{43}$ erg s$^{-1}$. Component 1: broken power law, 2:neutral absorber, 3,4: warm absorbers. All emission components are modified by Galactic photoelectric absorption.

| comp. | param. | R1+R2 | PN |
|---|---|---|---|
| 1 | $\Gamma_1$ | 2.8±0.1 | 2.71±0.07 |
| | $\Gamma_2$ | ... | 2.32±0.07 |
| | $E_{\rm break}$ (keV) | ... | 1.9±0.2 |
| 2 | $N_{\rm H}$ | 3.0±1.6 | 4.2±0.6 |
| 3 | $N_{\rm H}$ ($10^{20}$ cm$^{-2}$) | 24±5 | 15±3 |
| | $\log\xi$ | –0.9±0.2 | –0.8±0.3 |
| | $v_{\rm out}$ (km s$^{-1}$) | –1800±400 | –1800 fix. |
| 4 | $N_{\rm H}$ | 13±4 | 9±3 |
| | $\log\xi$ | 1.6±0.2 | 1.3±0.3 |
| | $\chi^2/\nu$ | 231/211 | 806/788 |
| | $F_{2-10\,\rm keV}$ | ... | 7.9±0.26 |
| | $F_{0.5-2\,\rm keV}$ | 8.46±1.34 | 8.1±0.5 |
| | $L_{2-10\,\rm keV}$ | ... | 7.47±0.25 |
| | $L_{0.5-2\,\rm keV}$ | 1.49±0.22 | 1.26±0.36 |

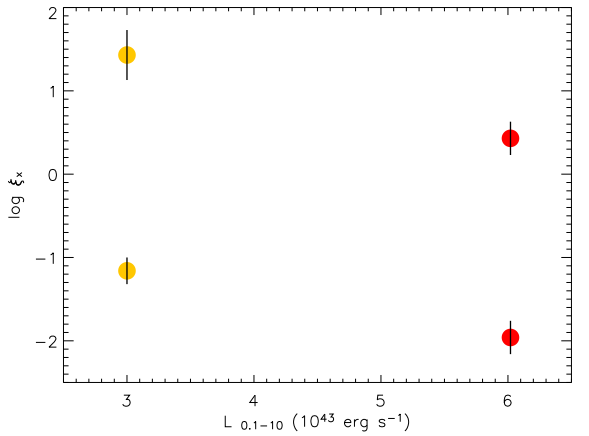


**Figure 7.** The log of the X-ray ionisation parameter, $\xi_{\rm X}$, against the 0.1–10 keV intrinsic luminosity for the 02 (dark dots) and 05 (light dots) components.

## 4 DISCUSSION

### 4.1 The X-ray warm absorber

The 02 and 05 spectra clearly show absorption by ionised gas. There were two detected components in 02, with ionisation parameters $\log\xi$= –0.9 and 1.6. The 05 spectrum was also well fitted with two warm absorber components, showing absorption with higher ionisation ($\log\xi \sim 0$ and 2.6). In Fig. 6 we plot the gas temperature ($T$) against the ionisation pressure parameter $\Xi$ for the 02 and 05 SEDs (drawn with the solid and dashed lines, respectively). The ionisation pressure parameter is defined as $\Xi \equiv L/4\pi r^2 cp$, where $L$ is the ionising luminosity, $r$ the gas distance from the source, and $p$ the gas pressure. The dark dots mark the position of the 02 warm absorbers on the stability curve relative to the SED at that epoch, while the light dots are the components detected in 05. Our curves show a wide interval of $\log\Xi$ in which the absorbers exist in a cold regime. This is where the "cold" components 02a and 05a lie. The ascending part ($\log\Xi > 0.5$) of the curve does not present the typical turnover S-shape (e.g. Crenshaw et al. 1999). This is because of the relatively steep X-ray SED of I Zw 1 (Krolik et al. 1981; Guilbert et al. 1983). We note that both the two 02 and two 05 components lie far apart from each other and are not in pressure equilibrium. This behaviour has been observed in other Seyfert 1 galaxies (e.g., Steenbrugge et al. 2005; Costantini et al. 2007). This suggests that conditions other than pressure equilibrium (Krolik Kriss 1995) should be present to make the two absorbers co-exist, such as magnetic confinement, as already suggested for the broad line region clouds (e.g. Rees 1987). The lower ionisation $a$ components show an outflow velocity of roughly 1700-1800 km s$^{-1}$ in 02 and 05. Therefore there are no strong velocity changes apparent over time, although the constraints on velocity changes are limited.

### 4.2 Long-term changes in the warm absorbers

The X-ray ions are mostly influenced by the 0.1–10 keV radiation, rather than by the UV photons (e.g. Netzer 1996). Therefore in the discussion below we shall use the X-ray ionisation parameter $\xi_{\rm X}$, obtained simply by scaling down the ionising luminosity to the 0.1–10 keV band (e.g. George et al. 1998). This calculation can be done only for the *XMM-Newton* data sets, for which the complete ionising SEDs were available. The values for $\xi_{\rm X}$ then become $-1.96 \pm 0.2$ and $0.43 \pm 0.22$ for the 02a and 02b components, respectively. The 05a and 05b values are $-1.16 \pm 0.16$ and $1.43 \pm 0.3$, respectively. In Fig. 7, $\xi_{\rm X}$ of both the 02 and 05 components are plotted against the 0.1–10 keV luminosity. Note that in general the ionisation parameter value is SED dependent. For the 02a and 05a components the corresponding stability curves (which are mostly dependent on the SED shape, Bottorff et al. 2000) are indistinguishable (Fig. 6). The stability curves start to differ slightly at higher values of $\Xi \propto \xi/T$, therefore we compare the 02b and 05b results with this caveat in mind. We note a significant anti-correlation between the 0.1−10 keV luminosity and the X-ray ionisation parameter. For a twofold decrease in luminosity between 02 and 05, the low ionisation (*a* components) $\xi_{\rm X}$ *increases* by a factor of $\sim 6.2$. For the 02b and 05b components, the increase factor is $\sim 10$. We may consider the *a* and *b* absorbers of 02 and 05 to be low- and high-ionisation components. If the observed ionisation comes from gas in equilibrium, we should invoke either a decrease in density (i.e. the gas thickness should increase, as $N_{\rm H}$ did not change dramatically) between 02 and 05, or movement of the gas *closer* to the central source. The latter seems an unlikely possibility as blue-shift of the *a* components is observed in 02 and 05. If the gas consists of discrete outflowing narrow filaments or clouds, then we do not expect to see the same structure along our line of sight if the distance $\Delta r$ travelled by this gas is much larger than its characteristic size $d$. For a rest-frame time difference of ∼1057 days between both observations and the measured outflow velocity of 1700 km s$^{-1}$, $\Delta r \sim 1.5 \times 10^{16}$ cm.
For the following calculation we consider the case $\Delta r \gtrsim d$, i.e. the size of the cloud is comparable to the gas travel path. The absolute distance of the centre of the cloud $r$ from the source should be much larger than the sizes considered here, therefore we also assume that the change in $r$ is not a critical term. We then compute

$$\frac{\xi_{05}}{\xi_{02}} = \frac{L_{05}}{L_{02}} \times \left(\frac{N_{\rm H}}{d}\right)_{02} \times \left(\frac{d}{N_{\rm H}}\right)_{05},$$

where $nd = N_{\rm H}$. The observed $\xi_{\rm X}$ ratio between 05 and 02 is 7 for the *a* components. The X-ray luminosity ratio is 0.5. With a simple calculation we obtain $d_{05}/d_{02} = 7.6$. Keeping in mind the assumption $\Delta r > d_{02} \sim 1.5 \times 10^{16}$ cm, for the *a* components we obtain $n_{02} < 1.6 \times 10^5$ cm$^{-3}$ and $n_{05} < 1.1 \times 10^4$ cm$^{-3}$. These are very low values compared to the estimated limits for the warm-absorber densities $2 \times 10^6 - 10^9$ cm$^{-3}$ (Netzer et al. 2002; Kraemer et al. 2002), therefore it seems unlikely that we are observing the same portion of the gas in both 02 and 05.
A scenario that could reproduce the observed anti-correlation sees the gas constantly in a non-equilibrium state (e.g. Nicastro et al. 1999) because, for example, of a delay in the gas response. Such a delay may be due to the gas having a very low density ($10^{7-8}$ cm$^{-3}$, Nicastro et al. 1999). Alternatively, the outflowing gas may be "transient", in the form of clouds or filaments passing through the line of sight. A variety of distinct ionisation stages, seemingly unrelated to the ionising flux, could be then accounted for. This explanation is strengthened if, contrary to what is observed for I Zw 1, components with very different column densities were observed at different times (e.g. Kraemer et al. 2001, 2005; Costantini et al. 2000). The outflow velocity may not change in time, if the gas is also moving transversely (Crenshaw et al. 2003; Kraemer et al. 2005). Finally, the anti-correlation seen in Fig. 7 may be the result of a shielding of the gas which is thus experiencing a filtered ionising luminosity. Qualitatively, the (self-)shielding of the gas may happen away from our line of sight, and is not directly observable in a complex gas environment as depicted for example in Proga (2005); Proga Kallman (2004) for the UV and X-ray emitting regions.

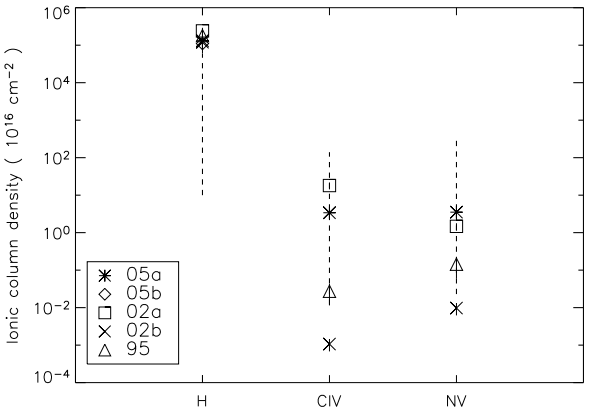


**Figure 8.** Column density of hydrogen (H I+H II), N V and C IV predicted by the X-ray absorbers at different epochs. The dashed vertical lines show the range of $N_{\rm H}$ inferred from the HST measurements taken in 1994 (Laor et al. 1997).

### 4.3 The connection with the UV absorber

Some of the gas components detected in the X-rays might also absorb in the UV band. In the HST spectrum of I Zw 1, obtained in 1994 (Laor et al. 1997), the presence of N V and C IV absorption features with an outflow velocity of $-1870$ km s$^{-1}$, clearly highlighted the presence of a warm absorber. Unfortunately the column densities of the absorption troughs were poorly determined in the HST spectrum: $\log N_{\rm CIV} = 14.07 - 18.14$ and $\log N_{\rm NV} = 14.36 - 18.51$. The derived total hydrogen column density was $\log N_{\rm H} = 17 - 20.77$. The UV measurements (displayed with the dashed vertical lines) are compared in Fig. 8 with the values obtained in the X rays at different epochs. The ionic column densities of N V and C IV, which are visible only in the UV band because of their low ionisation, were derived from the best-fit models of the X-ray absorbers. The *a* X-ray components have values of $N_{\rm NV}$ and $N_{\rm CIV}$ which are compatible with the UV column densities. Also the ASCA column density measurements are consistent with the UV values, while

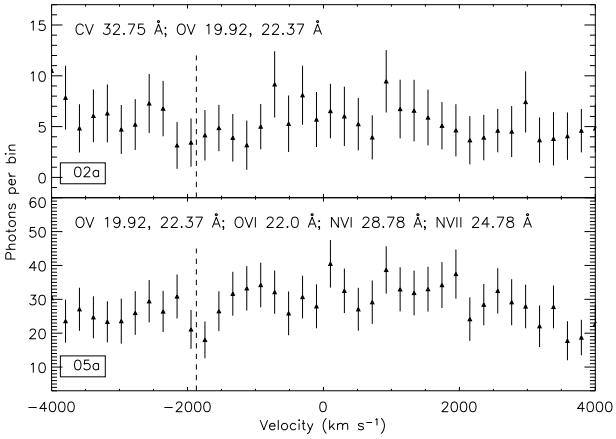


**Figure 9.** *XMM-Newton* velocity spectra for the 02a (upper panel) and 05a (lower panel) components. The bin size is $200\,\mathrm{km\,s^{-1}}$. The transitions chosen to produce the stack of the (unblended) line profiles for each absorber are also labelled. The vertical dashed line marks the blue-shift as measured by HST-FOS. Note that the redshift used in the HST analysis was 0.0608 which implies a shift in the outflow velocity of only $90\,\mathrm{km\,s^{-1}}$, which is negligible compared to the errors associated to the X-ray measurements.

the *b* components clearly do not produce enough of these low-ionisation ions. Interestingly, the UV flux in 1994 was about four times higher than in 02 and 05. This at least suggests that a low ionisation outflowing component may survive years, despite large changes in the UV flux (and presumably of the overall level of the SED). The UV total hydrogen column density is slightly lower than for the X-ray absorbers (Fig. 8). The outflow velocity measured from the X-ray spectra is consistent with the value found in the HST-FOS spectrum. This is shown in Fig. 9 where the velocity spectra for the 02a and 05a components are compared (see e.g. Kaspi et al. 2002, for details on the procedure). The vertical dashed line marks the blue-shift as measured from the UV N v line ($-1870\,\mathrm{km\,s^{-1}}$; Laor et al. 1997). The outflow velocity of the UV-X-ray gas did not change in time, within uncertainties. This suggests that we are observing a gas not dramatically influenced by changes of the central source (e.g. changes in the acceleration of the flow, or strong variability of the source). Therefore the observed gas may be in the terminal-velocity portion of the flow, at a considerable distance from the central source, for example at a parsec scale, produced either by evaporation in a molecular torus (Krolik Kriss 2001), or by instabilities of the outer rim of the accretion disc, which in principle can extend to large distances. As a note of caution, the comparison between the X-ray and the UV absorbers discussed here is based on non-simultaneous data, which may be misleading (Crenshaw et al. 2003). In addition, the UV information given by HST gives only partial information on the SED, which would be important for an unambiguous comparison between the UV and X-ray bands.

## 5 CONCLUSIONS

We have presented the *XMM-Newton* low-energy X-ray data of I Zw 1, collected in 2005. In the absorbed spectrum we find evidence of a neutral phase, stable at least over the last ten years and probably associated with the host galaxy or with the interaction stream to the companion galaxy of I Zw 1 (see also Paper I). In addition, two ionised absorption components with similar column densities of $\sim few \times 10^{21}$ cm$^{-2}$ and ionisation parameters $\log \xi \sim 0$ and 2.5 are detected. Comparing these results with a previous *XMM-Newton* observation and archival ASCA and HST data we conclude:

- The two ionised gas components detected in both 05 and 02 cannot be in pressure equilibrium with each other. For the two components to coexist, a different mechanism, like magnetic confinement and/or gas shielding has to play a role.
- The X-ray ionisation parameter $\xi_{\rm X}$ is clearly anti-correlated with the X-ray luminosity. A viable explanation for this considers a gas organised in filaments crossing the line of sight. However the similarity of the column densities of the *a*, *b* components and also of the gas detected in the ASCA spectrum, make this possibility not as clear as for other cases (e.g. NGC 4151, Kraemer et al. 2005). Other possibilities, like a non-equilibrium state of the absorber, would need continuous monitoring to be rigorously tested. Finally, we may think that the observed gas might be shielded from the continuum source in the context of a complex and turbulent gas environment and experience a filtered ionising flux.
- The gas producing the X-ray lower ionisation absorbers detected in 02 and 05 can also produce the low-ionisation species (N v and C iv) seen in the HST spectrum (Laor et al. 1997), as the column densities and outflow velocities are consistent. Interestingly however, the UV absorber was observed when the UV flux was about 4 times higher than the ones recorded by *XMM-Newton*-OM. This shows that a low ionisation component can survive for at least ten years, despite significant variations in the UV flux. The constant outflow velocity of the UV and the X-ray absorbers in time suggests also that we are observing the terminal velocity portion of the gas, probably located at a large distance from the source. The caveat is that the X-ray-UV comparison is performed with non-simultaneous observations, which might be misleading.

## 6 ACKNOWLEDGEMENTS

We thank Jelle Kaastra for useful discussion. The Space Research Organisation of the Netherlands is supported financially by NWO, the Netherlands Organisation for Scientific Research. WNB acknowledges support from NASA LTSA grant NAG5-13035 and NASA grant NNG05GR05G. This research has made use of the Tartarus (Version 3.1) database, created by Paul O'Neill and Kirpal Nandra at Imperial College London, and Jane Turner at NASA/GSFC. Tartarus is supported by funding from PPARC and NASA grants NAG5-7385 and NAG5-7067.

**REFERENCES**


Anders E., Grevesse N. 1989, Geocosmochimica Acta , 53, 197
Behar E., Sako M., Kahn S. M. 2001, ApJ, 563, 497
Boller T., Brandt W. N., Fink H. 1996, A&A, 305, 53
Bottorff M. C., Korista K. T., Shlosman I. 2000, ApJ, 537, 134
Condon J. J., Hutchings J. B., Gower A. C. 1985, AJ, 90, 1642
Costantini E., et al. 2000, ApJ, 544, 283
Costantini E., et al. 2007, A&A, 461, 121
Crenshaw D. M., Kraemer S. B., Boggess, A. Maran, S. P., Mushotzky R. F., Wu C.-C. 1999, ApJ, 516, 750
Crenshaw D. M., Kraemer S. B., George I. M. 2003, ARA&A, 41, 117
Crenshaw, D. M., et al. 2003, ApJ, 594, 116
Crummy J., Fabian A. C., Gallo L., Ross R. R. 2006, MNRAS, 365, 1067
den Herder J. W., et al. 2001, A&A, 365, L7
Elvis M., Wilkes B. J., Lockman F. J. 1989, AJ, 97, 777
Ferland G. J., Martin P. G., van Hoof P. A. M., Weingartner J. C. 2002, X-ray Spectroscopy of AGN with Chandra and XMM-Newton, 103
Ferland G. J. 2004, Bulletin of the American Astronomical Society, 36, 1574
Gallo L. C., Boller T., Brandt W. N., Fabian A. C., Vaughan S. 2004, A&A, 417, 29
Gallo L. C., Brandt W. N., Costantini E., Fabian A.C., Iwasawa K. Papadakis I.E. 2007a, MNRAS, accepted, astro-ph/0610283 (Paper I)
Gallo L. C., Brandt W. N., Costantini E. Fabian A.C. 2007b, MNRAS, submitted
George I. M., Turner T. J., Mushotzky R., Nandra K., Netzer H. 1998, ApJ, 503, 174
Guilbert P. W., McCray R., Fabian A. C. 1983, ApJ, 266, 466
Halpern J. P., Oke J. B. 1987, ApJ, 312, 91
Kaastra J. S., Barr P. 1989, A&A, 226, 59
Kaastra J. S. et al. 2002, A&A, 386, 427
Kaspi S., et al. 2002, ApJ, 574, 643
Kraemer S. B., Crenshaw D. M., Gabel J. R. 2001, ApJ, 557, 30
Kraemer S. B., Crenshaw D. M., George I. M., Netzer H., Turner T. J., Gabel J. R. 2002, ApJ, 577, 98
Kraemer S. B., et al. 2005, ApJ, 633, 693
Kriss G. A. 2002, ASP Conf. Ser. 255: Mass Outflow in Active Galactic Nuclei: New Perspectives, 255, 69
Krolik J. H., McKee C. F., Tarter C. B. 1981, ApJ, 249, 422
Krolik J. H., & Kriss G. A. 1995, ApJ, 447, 512
Krolik J. H., Kriss G. A. 2001, ApJ, 561, 684
Laor A., Jannuzi B. T., Green R. F., Boroson T. A. 1997, ApJ, 489, 656
Lawrence A., Elvis M., Wilkes B. J., McHardy I., Brandt N. 1997, MNRAS, 285, 879
Leighly K. M. 1999, ApJS, 125, 317
Mason K. O., et al. 2001, A&A, 365, 36
Mathur S., Elvis M., Wilkes B. 1995, ApJ, 452, 230
Netzer H. 1996, ApJ, 473, 781
Netzer H., Chelouche D., George I. M., Turner T. J., Crenshaw D. M., Kraemer S. B., Nandra K. 2002, ApJ, 571, 256
Nicastro F., Fiore F., Perola G. C., Elvis M. 1999, ApJ, 512, 184
Otani C., et al. 1996, PASJ , 48, 211
Proga D., Kallman T. R. 2004, ApJ, 616, 688
Proga D. 2005, ApJ, 630, L9
Rees M. J. 1987, MNRAS, 228, 47P
Reynolds C. S. 1997, MNRAS, 286, 513
Ross R. R., Fabian A. C. 2005, MNRAS, 358, 211
Sargent W. L. W. 1968, ApJ, 152, L31
Steenbrugge K. C., et al. 2005, A&A, 434, 569
Strüder L., et al. 2001, A&A, 365, L18
Tananbaum H., et al. 1979, ApJ, 234, L9
Turner M. J. L., et al. 2001, A&A, 365, L27
Turner T. J., Kraemer S. B., George I. M., Reeves J. N., Bottorff M. C. 2005, ApJ, 618, 155
Vestergaard M., Wilkes B. J. 2001, ApJS, 134, 1